論文 / 著書情報
Article / Book Information

Title	Liquefaction-induced large displacement of pile-supported wharf
Authors	Akihiro Takahashi, Jiro Takemura
Citation	Soil Dynamics and Earthquake Engineering, Vol. 25, pp. 811-825
Pub. date	2005, 12
DOI	http://dx.doi.org/10.1016/j.soildyn.2005.04.010
Creative Commons	See next page.
Note	This file is author (final) version.

License

Liquefaction–induced large displacement of pile-supported wharf

Akihiro Takahashi* [1] & Jiro Takemura [2]

Abstract

Centrifuge model tests were carried out to investigate the dynamic behaviour of a pile-supported wharf in front of back-filled gravity type caissons, focusing on the failure mechanism of the piles, the effects of liquefaction in the backfill and underlying sand layer on the permanent deformation of the wharf during earthquakes, and the dynamic interaction between the piled deck and caisson through the approach bridge. The targeted piled structure is the pile-supported wharf damaged in the 1995 Hyogo-ken Nambu Earthquake at Takahama, Kobe. Liquefaction of the foundation soil and the backfill behind the caisson during an earthquake-like shaking causes large seaward lateral movement of the rubble mound. As a result, a large horizontal displacement gap was formed between the rubble mound and the bearing stratum. This displacement gap caused a very large bending moment in the pile, at the pile top and in the bearing stratum just below the sand layer. These locations where large bending moments were observed agreed with the locations where large pile deformations were observed at the Kobe site. Centrifuge model tests reasonably predicted the failure mode of the piled wharf observed in the Kobe Earthquake. Varying the thickness of the sand layer under the rubble mound caused a change of the deformation mode of both ground and structures. The test without the sand layer showed no displacement gap between the rubble mound and the bearing stratum, resulting in small permanent displacement of the wharf, while a thicker liquefiable sand layer did not necessarily cause a larger deformation of soil and the structures.

Soil Dynamics and Earthquake Engineering, 25(11), 811-825, 2005
Original URL:
http://dx.doi.org/10.1016/j.soildyn.2005.04.010

[1] Earthquake Disaster Prevention Research Group, Public Works Research Institute, Japan
[2] Department of Civil Engineering, Tokyo Institute of Technology, Japan

Introduction

One of the major sources of earthquake-induced damage to port facilities is liquefaction of saturated loose sandy soils. This type of soil often prevails at waterfronts and marine environments. The significant liquefaction and associated ground movement and waterfront structure damage have not only occurred under very strong earthquakes like the 1995 Hyogo-ken Nambu Earthquake, but also under moderate levels of earthquake motion in past earthquakes [1]. Near waterfronts many pile-supported structures, especially pile-supported buildings, had pile damage without severe damage to their superstructures in past earthquakes. During the lateral spreading of liquefied soil, the covering non-liquefied soil, i.e. the soil layer above the water table, moves seaward together with the liquefied soil. Pile foundations located in such a lateral spreading ground behind quay walls were investigated, and detailed observations revealed that the damage to the piles occurred at depths other than the pile heads, particularly near the interface between the liquefied and non-liquefied soils [2] [3].

Not only the piles behind the quay walls, but also those in front of the wall were damaged. For instance, the 1989 Loma Prieta Earthquake caused damage to the pile-supported wharves at the port of Oakland [1]. All of the piles of the wharves were installed into rock dikes. Dredged sands and silty sands were filled behind the dikes. A deck of the Seventh Street Terminal wharf was a ballasted cast-in-place concrete slab, and it was supported by vertical piles in six rows and battered piles in one row [4]. The hydraulic sand fill and the upper 1.5m of the dense native sand experienced liquefaction and the wharf moved 0.3m seaward during the Loma Prieta Earthquake. Most of the battered piles were cracked or fractured, though the vertical piles and the deck suffered only minor damage. The wharf and embankment strengthening program is undertaken at the port of Oakland to design and construct the structural modifications necessary to mitigate the effects of the deepening project in conjunction with a federal government-sponsored channel dredging project [5]. Salah-Mars *et al.* [6] reports seismic evaluation of the wharf and embankment at the port using FLAC and demonstrates effectiveness of (1) soil improvement in the backfill and embankment and (2) installation of a sheet pile wall at the toe of the embankment on mitigation of wharf permanent deformation.

Several piers and wharves were also damaged during the 1995 Hyogo-ken Nambu (Kobe) Earthquake [2] [7] [8] [9] [10] [11]. The wharf supported on vertical piles moved 1.3 to 1.7m toward the sea at Takahama in Kobe [8] [9]. The Takahama Wharf was constructed in front of stacked gravity type caissons made of concrete cellular blocks as shown in Fig. 1. The wharf was constructed on a firm foundation deposit that consists of alternating layers of Pleistocene clay and sandy gravel. The caissons were installed on a layer of loose sand layer about 2m thick, and hydraulically backfilled with the decomposed granite, *masado*. The concrete deck of the wharf was supported by three rows of steel pipe piles with a diameter of 700mm and connected to the top caisson with approach bridges. Thicknesses of the steel pipe piles were 10, 12 and 14mm from sea-side to land-side, respectively. The piles of the deck penetrated the sand layer into the bearing strata consisting of gravel and Pleistocene clay layers. The rubble mound was constructed on the sand layers in order to increase lateral resistance of the deck against shiploads.

After the Hyogo-ken Nambu Earthquake, a detailed investigation on the damaged wharf was carried out, including post-mortem observations of the piles. Clear failures with bending were observed in the removed piles. Large deformations took place at the top, near the deck of the wharf, and at the interface between the rubble mound and the liquefiable sand layer, as shown in Fig. 1. Also, several cracks were found on the approach bridges and the connection points between

the bridges and the deck of the wharf.

Using shaking tables in geotechnical centrifuges as well as ordinary shaking tables, many researchers have experimentally investigated the effects of the large lateral soil movement – especially liquefaction-induced lateral spreading of soil – on the failure and deformation of the piles on slopes and behind the quay walls. However, only a limited number of shaking table tests have been carried out for pile-supported wharves [12] [13] [14] [15] [16] [17], although many questions remain in the seismic performance of wharves, i.e. pile-failure mechanism, effects of liquefaction in backfill and sand layer on permanent deformation of the wharf, and dynamic interaction between deck and caisson through the approach bridge. In order to examine wharf response during an earthquake in detail paying attention to above-mentioned several factors affecting the wharf response, the authors has carried out physical model tests using a geotechnical centrifuge. In addition, since enough space could not be secured in front of the wharf and in the backfill behind the caisson in the centrifuge model tests due to the limitation of the container size, effects of the model container size, i.e. side boundary conditions, on permanent deformation of the wharf as well as the model ground were examined by two-dimensional numerical analyses without the piled deck.

Centrifuge model test procedures and conditions

The centrifuge used was the Tokyo Tech Mark II Centrifuge [18]. The model setup used is shown in Fig. 2. An aluminium model container was used with inner sizes of 450mm in length, 150mm in width, and 250mm in height. The inner side of the container was coated with alumite. The front face of the container was a transparent glass window that enabled observation of the model's ground deformation. Rubber sheets 10mm thick were placed at both sides of the container to absorb stress waves from the side boundaries. Due to the limitations of the container size and a 50g allowable centrifuge acceleration for shaking test, prototype scales of all dimensions of the model were reduced to half those of the site, and some simplifications were introduced in modelling the caissons and soil layers. The model piled deck consisted of an aluminium deck weighing 0.42kg and 9 piles rigidly fixed to the deck. The pile spacing ratio s/d=6.7, as shown in Fig. 3. The model piles were steel tubes having an outside diameter of 7mm, a thickness of 0.14mm, and a total length of 200 or 220mm (for PW7 only). Properties of the model pile are listed in Table 1. Strain gauges were instrumented inside each pile at 9 different levels. However, due to a limited number of data acquisition channels, data from only three or four gauges for each pile were used, as shown in Fig. 2. The piles of the deck were installed in three different soil layers; (1) a bottom dense sand bearing stratum corresponding to the gravel and Pleistocene clay at the Kobe site, (2) a saturated loose liquefiable sand layer, and (3) a top rubble mound. These soils were prepared by air pluviation. The basic properties of the soils used are summarised in Table 2. Aluminium gravity type caissons were placed between the rubble mound and the backfill. The unit weight of the caissons was 2.5kN/m^3. An approach bridge made of aluminium was placed between the deck and the caisson to transmit only compressive axial load. The bridge was placed in notches on the deck and the upper caisson. High viscosity fluid was usually used as pore fluid to avoid conflict with the scaling laws associated with the time of dynamic events and the seepage in centrifuge tests [19] [20]. Sand layers were saturated with a methyl-cellulose-base solution [21] which has a viscosity 50 times higher than that of water under a negative pressure of about 98kPa in a large tank by applying a vacuum. Ground water level was set at a depth of 40mm from the backfill surface in all the tests. Japanese noodles *somen* were placed between the model ground and the transparent window as

markers to observe deformation of the ground.

Table 3 gives the test conditions. In case PW1, a shaking test was conducted under 50g by applying the earthquake motion recorded at Kobe Port Island in 1995 to the shaking table (Fig. 4). This wave was recorded at a depth of 83m from the ground level, the same stratum as the bearing stratum for the wharf. As the wharf faced at an angle of 20 degrees to the north, the input motion was calculated using the NS- and EW-oriented ground accelerations. In the figure the input signal to the shaker was plotted with a dotted line, and the recorded motion of the table was plotted with a solid line. As shown in Fig. 4, the strong ground motion like the Hyogo-ken Nambu Earthquake could not be obtained in the simulation by the shaker used, although the differences in the displacement time history and the shape of the Fourier spectrum graph were not large. Hence, in cases PW2 through PW7, 20 sinusoidal waves with a frequency of 100Hz (2Hz in the prototype scale) were applied which approximated the spectral peaks of the recorded wave at Kobe P.I. around 70 and 140Hz (around 1.4 and 2.8Hz in the prototype scale). Typical time histories of the input sinusoidal waves are given in Fig. 5, together with its Fourier spectrum.

Besides PW1 and PW2, which simulate the conditions of the Kobe site, five additional tests were conducted. The stabilising effect of the deck piles on the lateral spreading of soils will be addressed in PW3 using a model without a deck. Assessment of the container size effects on the ground deformation will be made in the numerical simulation of PW3. In PW4 and PW5, to gain further insight into the effect of liquefaction on the large deformation of the wharf, the liquefiable sand layers under the rubble mound and behind the caisson were replaced by higher hydraulic conductivity silica sand to avoid liquefaction. The effect of the approach bridge on a dynamic interaction between the deck and the caisson will be discussed by comparing PW6 and PW2. In PW7, the thickness h_s of the liquefiable sand layer under the rubble was twice as large as that in PW1 and PW2. In order to align the embedded length of the pile into the bearing stratum in all the cases, piles with lengths of 220mm were used in PW7.

Due to the limited number of data acquisition channels, the number of instrumented locations were varied according to the test case as summarised in Table 4. Displacements of the deck and the lower caisson were measured by laser displacement transducers. These displacements were not measured directly on structures but at targets 30mm above the surface of the deck as shown in Fig. 2. All the physical values presented in the following sections are in the model scale.

Assessment of container size effects on test results by numerical analysis

Ground response without piled deck in physical model test

Figure 6 shows observed excess pore water pressures at cell locations P5, P2 & P6 in case PW3. The effective over burden pressures, σ'_{v0}, are also plotted in the figure. The pore pressure at P2, located in the liquefiable sand layers, levelled off at an early stage of the shaking although it did not reach σ'_{v0}. That at P6, located in the backfill, gradually increased with shaking and reached its σ'_{v0}. As the rubble had a higher hydraulic conductivity compared to the liquefiable sand layer, accumulation of the excess pore water pressure at P5 was very small. Taking this into account, the decrease in stiffness and strength of the rubble mound was thought to be small. The observed permanent deformation of the model ground in PW3 is shown in Fig. 7. As mentioned above, since the rubble mound was relatively stiff, the loss of the strength at the sand layer under the rubble could allow the caissons to move laterally seaward. As a result, a large horizontal displacement gap was observed between the rubble mound and the bearing stratum.

Numerical analyses with different model container width

The side walls of the model container could restrain the deformation of the model ground, and this deformation restriction resulted in the seabed heaving and the excessive backfill subsidence just behind the quay wall as shown in Fig. 7. In order to examine the model container size effects on permanent deformation of the quay as well as the model ground, two-dimensional numerical analyses without the piled deck were conducted. Details of the numerical code used in this study are described by the first author [22] [23].

In the analyses, the width of the model container was varied. One is the model whose width (W) is the same as that of the centrifuge model tests (W=440mm, 22m in the prototype scale), and the other is the model with double the width (W=880mm, 44m in the prototype scale). The finite element mesh used for W=440mm is shown in Fig. 8.

The extended subloading surface model proposed by Hashiguchi & Chen [24] was adopted for the soil layers. Material parameters of the soil layer and the pile are listed in Table 5, where G_s = specific gravity, e_0 = initial void ratio, κ & λ = slopes of swelling & compression lines in $v - \ln(p')$ plane, ν = Poisson's ratio, σ'_{ij0} = initiail stress, $\sigma'_{m0} = \sigma'_{ii0}/3$, δ_{ij} = Kronecker's delta, k=hydraulic conductivity, ρ = unit weight, E = Young's modulus, I = flexural rigidity of beam, A = area of beam section, and the other parameters are specific parameters for the constitutive model used. These parameters were determined so that single numerical simulations fitted cyclic undrained triaxial tests. Ellipsoid type surface is utilised for the yield and the subloading surfaces.

Nodes at the both ends of analytical domain were allowed to move freely in vertical directions but not in horizontal direction. At the bottom end, all movements were restrained. Fluid flow velocities were set to zero at all the boundaries except at the surface of the ground. A simple two-step loading of gravity was adopted in the static analyses to estimate the stress condition prior to the dynamic response analyses: In the first step, a stress analysis was conducted with the assumption that a deformation modulus of each soil is uniform irrespective of the confining pressure. (Typically, the modulus at the mid-depth of the soil layer is adopted in each soil.) Then, in the second step, the stress analysis was carried out with the stress-dependent deformation modulus using the stress condition obtained in the first step.

Applied earthquake motion was the acceleration record in the centrifuge test. In order to obtain the numerical solution, the differential equations were integrated along time. The integration scheme used was Newmark's β method, and the time step for the integration was Δt =0.0002sec. System damping was represented by Rayleigh damping, and the damping ratio used was 1% in a first mode of free vibration of the system. The first vibration period of the system was 0.0048sec.

Time histories of excess pore water pressure at P5, P2 & P6 are plotted in Fig. 9. The excess pore water pressure response for W=440mm and W=880mm are comparable, though at P6, which is located in the backfill, relatively lager fluctuation was observed in the W=440mm case. Although in the numerical analyses accumulation of the pressure was rather quick and the pressure slowly dissipated after shaking at P6 in comparison with the centrifuge model test (Fig. 6), the numerical analysis can capture the overall excess pore water pressure response.

Calculated horizontal displacements of the caisson at the target height, which is 30mm above the caisson surface as in the centrifuge test, are shown in Fig. 10. Unfortunately, since horizontal displacement of the caisson could not be recorded by the laser displacement transducer in PW3, only the permanent displacement of the caisson obtained from comparison of the photographs taken before and after shaking is indicated by the arrow in the figure. The caisson responses for W=440mm and W=880mm were very similar, resulting in more or less the same permanent displacement. In Fig. 11, permanent horizontal displacement distributions of the rubble mound level (z = 120mm) and the sand layer under the

rubble ($z = 80$mm) are plotted for both cases together with physical model test result (PW3). The displacements for the physical model test were obtained from the movements of the noodle targets placed between the transparent window of the container and the model grounds. Though the permanent horizontal displacements in the centrifuge test are smaller than those in the numerical analyses, the distributions are similar as a whole.

Figure 12 shows the permanent deformations of the model ground, together with the result for W=880mm with flexible side boundaries. The displacement scale in the figure is magnified by a factor of two. In the case with flexible side boundaries, responses of horizontally layered gound were input to the side boundaries, while nodes at the side boundaries were allowed to move freely in vertical directions but not in horizontal direction in the other cases.

In the cases of rigid side boundaries, the large seabed heaving and backfill settlement were observed in the case of W=440mm, while the heaving and the settlement in the case of W=880mm were small. As seen in Fig. 12(c), marked effects of side boundary conditions on the permanent displacement of the quay wall and the rubble mound cannot be seen, although the rubble mound displacement for the case with the flexible side boundaries is slightly smaller than that for the rigid side boundaries case.

The quay wall and the rubble mound showed essentially the same permanent displacement in all the cases. This fact supports the conclusion that the wharf responses obtained in this study were not much affected by the side walls of the model container, while the distances of the model container side walls from the quay heavily influence the deformation of the ground, since the quay movement is the cause and the deformations of the backfill and the seabed are the consequence. Therefore, determining the width of the domain behind the quay is more important and much affects the piled structure responses when the targeted piled structure is located behind the quay.

Although the ground movement in front of the quay is relatively less affected by the sea-side boundary as seen in the figures, differences still exist; the narrower rigid container tends to give us slightly smaller horizontal displacement of the wharf and the displacement for the case with the flexible side boundaries is slightly smaller than that for the rigid side boundaries case. Thus, it should be noted here that the wharf horizontal displacement in the field could be different from those seen in the centrifuge. However, the results from one test can be compared to others as all the centrifuge tests were undertaken in the same model container.

Simulation of the Takahama Wharf damaged in the 1995 Hyogo-ken Nambu Earthquake

Figure 13 shows observed excess pore water pressures at cell locations P2 & P4 and accelerations at meter location A6 in cases PW1 and PW2. The effective over burden pressures, σ'_{v0}, are also plotted in the figure. In case PW1 the excess pore water pressure at P2 almost reached a value of 80% of its σ'_{v0} at two peaks in the input wave, i.e. at 0.04 and 0.12 seconds, but full liquefaction was not observed in this case. In PW2, the pore pressure at P2, located in the liquefiable sand layers, reached σ'_{v0} and levelled off, showing liquefaction at an early stage of the shaking. Although excess pore water pressure at P6 was not recorded in PW2, the backfill was seen to be liquefied, considering that the acceleration response at A6 was remarkably attenuated with shaking in PW2, and the pore pressure at P6 in PW3 reached its σ'_{v0} as shown in Fig. 6. As mentioned in the previous section, the decrease in stiffness and strength of the rubble mound was thought to be also small in PW2, since accumulation of the excess pore water pressure at P5 in PW3 was very small.

The observed permanent deformation of the model ground in PW2 is shown in Fig. 14. The structures moved laterally seaward, and a large horizontal displacement gap was observed between the rubble mound and the bearing stratum as seen in PW3 (Fig. 7). (Permanent deformation of the model ground in PW1 was essentially the same as that observed in PW2, although the displacement was smaller than that in PW2.) Although rows of piles are sometimes used for stabilisation of a moving slope, i.e. a landslide, and this stabilising effect of the rows of piles might have a potential for preventing the movement of the rubble mound and/or the caisson, it could not be seen in this study. Figure 15 shows permanent lateral displacements of the rubble mound and the sand layer under the rubble in PW2 and PW3. Regarding the pile spacing of the deck, the movement of the front side of the model ground corresponded to that at the centre of the pile space. Although obtained data are scattered, the displacement distributions of the rubble and the sand layer are nearly the same, and no remarkable difference can be seen since the pile spacing ratio was relatively larger than that of the other types of piled structure.

Figure 16 illustrates observed lateral displacements of the deck and the lower caisson. It should be noted that the displacements shown in the figure were not measured directly at those structures but at targets 30mm above the surface of the deck as shown in Fig. 2. Regarding the plot of the lower caisson (dotted line in Fig. 16), the laser displacement transducer went out of its measurable range as the target surface defected its laser reflection. It is apparent from the figure that the caisson and the deck moved together in the early stages of the shaking. Displacements of the caisson, however, became larger than that of the deck, which may have been caused by the relatively large tilting of the caisson. In PW1, permanent displacements of the structures were smaller than those in PW2. Two large fluctuations were observed, corresponding to the peaks of input acceleration. The structures gradually moved with time, and no substantial displacement took place after the shaking in PW2. This result suggests that not only deterioration of the soil strength due to liquefaction but also the continuous cyclic force had substantial effects on the accumulation of the deck displacement.

For case PW2, the bending and axial strains on the piles at various depths were measured, and the values recorded just after the shaking are shown in Fig. 17. Also for case PW2 the variation of strains measured at the top (St9S & St9L), at the sand layer (St4S & St4L), and at the bearing stratum just below the sand layer (St2S & St2L) for the sea-side and the land-side piles are illustrated in Fig. 18 together with the axial strain variations at the pile head. As strain gauges were put only on the right inside of the piles, outputs from them include strains caused by axial tension or compression as well as bending. However, the variation of the axial strain measured by two parallel strain gauges was very small compared to the measured strain on the right side of the pile, as shown in Fig. 18. The measured strain on the right side of the pile would be nearly equal to the bending strain of the pile. Negative values in the figure represent compression on the right side of the pile. As shown in this figure, a very large negative strain appeared at the top of the piles, and large positive values were measured in the bearing stratum just below the sand layer, also evident in Fig. 17. These points agree with the locations of large pile deformation observed at the Kobe site as illustrated in Fig. 1. All indications support the conclusion that the centrifuge model tests can reliably show us the failure mode or mechanism of the wharf at the actual site. The strain on the piles changed sign in the sand layer irrespective of the pile row. This fact represents that the inflection points in the piles deflection existed at this level, and there was large relative displacement between the rubble mound and the bearing stratum as shown in Fig. 14. The deck moved seaward as a result of lateral movement of the rubble mound and behaved as a *passive pile*.

Regarding the amplitudes and accumulations of strain on the pile, the strains observed at the pile head (St9S & St9L)

are larger than those at the bearing stratum just below the sand layer (St2S & St2L), especially in the early stage of shaking. Both the larger amplitude and the larger permanent strain at the top of the piles suggest that the large deformation at the pile head initiated the failure of the deck pile before that at the lower portion of the pile around the sand layer under the rubble mound. According to the results of a beam structure analysis of the deck subjected to rubble mound movements through soil springs by Minami *et al.* [8], the structure hinging initially occurred at the heads of the sea-side and the land-side piles and at the lower portion which corresponded to the depth of the liquefiable layer of the middle pile, and then the hinging came to the lower portion of the sea-side and the land-side piles. The centrifuge test results agree with their analysis results as a whole, although there are minor differences in the middle pile response and the bending strains don't reach their elastic limits. In the following sections, effects of several factors on the permanent deformation of the wharf will be discussed.

Deck–caisson interaction through approach bridge

The wharf deck in this study was connected to the caisson by the approach bridge. As mentioned above, cracks were found on the approach bridges and the land-side of the deck at the Takahama Wharf. These cracks were seen to be caused by clashing between the bridge and the deck. Though the impact was not enough to collapse the deck, the interaction between the deck and the caisson through the approach bridge might increase the damage to the wharf. In order to examine effects of the approach bridge on the permanent deformation of the wharf, a centrifuge test result without the approach bridge (PW6) will be compared with a test with the bridge (PW2).

Observed displacements of the deck in PW2 and PW6 are shown in Fig. 19. Comparing the results in PW2 and PW6, the velocity of the deck in PW6 was smaller than that in PW2, resulting in smaller permanent displacement. Accelerations observed at the deck in PW2 and PW6 are compared in Fig. 20. Acceleration in the seaward direction is taken as positive in the figure. In PW2, clear spikes can be seen in the positive peaks where the deck moved landward. This implies that the landward movement of the deck was prevented by the caisson through the approach bridge, and a large horizontal force was applied from the caisson. It can be expected that the approach bridge accelerated the seaward movement of the wharf.

Liquefaction of sand layers

Liquefaction of the sand layers undoubtedly affected the permanent deformation of the wharf. Although this fact can be qualitatively accepted, how the liquefaction of the sand layers quantitatively affects performance of the wharf is unknown. In order to examine the liquefaction effects on the wharf performance, in PW4 and PW5 the liquefiable sand layer under the rubble mound (PW4) and behind the caisson (PW5) were replaced by higher hydraulic conductivity silica sand to avoid liquefaction. The density of the replaced soil was adjusted to that of the original liquefiable layer. In order to study the effect of the thickness of the liquefiable sand layer under the rubble mound, the thickness (h_s) of the liquefiable sand layer under the rubble in PW7 was twice as large as that in PW1 and PW2.

Observed excess pore water pressures at P2 in PW4 and at P4 in PW5 and acceleration at A6 in PW5 are illustrated in Fig. 21. Responses of pore pressures and acceleration in PW2 are plotted in dotted lines for comparison. Although excess pore water pressures at P2 in PW4 and at P4 in PW5 (where the liquefiable sand was replaced by high hydraulic conductivity sand) showed almost the same response as those in PW2 in the early stages, quick dissipation of pore

pressures was observed. Such dissipation was not marked in the other tests. The amplitude of the acceleration at A6 remained constant with the shaking in PW5, while the acceleration response was remarkably attenuated in PW2. These facts show that the replacement of the liquefiable soil performed well as a countermeasure.

Observed horizontal displacements of the lower caisson and the deck in PW2, PW4, PW5 & PW7 are shown in Fig. 22. In the early stage of the shaking, the responses of the deck and the caisson were almost the same and they moved together in all the cases. Except in PW7, the displacements of the caisson, however, became larger than that of the deck, which may be caused by the relatively large tilting of the caisson, as previously explained. In PW7, the tilting of the caisson was small, and the horizontal displacement of the deck and the caisson was almost the same, as shown in Fig. 23.

Displacements of the deck and the caisson in PW4 and PW5 were smaller than those in PW2. Comparing the results in PW4 and PW5, the velocity of the structures in PW4 decreased at earlier stages than in PW5, resulting in smaller displacements. Under these test conditions, it can be concluded that the liquefaction at the sand layer beneath the rubble mound and caisson has more marked effects on the movement of the structures than that at the backfill.

Observed deformations of the model ground due to the shaking in PW2, PW4, PW5 and PW7 are shown in Figure 23. The horizontal displacement gap between the rubble mound and the bearing stratum was remarkably smaller in PW4 than the other cases. Considering the fact that liquefaction took place in the sand layer between these two layers except in PW4, as shown in Fig. 21, it can be said that even the thin sand layer under the rubble mound, i.e. 1–2m in these model tests and at Takahama, had a significant effect on the displacement of the rubble mound and caisson. Regarding the difference in the thickness of the liquefiable sand layer under the rubble, significant settlement of the caisson and squeezing of the sand layer between the two non-liquefiable layers were observed in PW7, while in PW2 displacement of the rubble mound was larger than that of the sand layer, and no large settlement was observed. This result indicates that variation of the thickness of the sand layer under the rubble mound causes a change of deformation mode of the ground and structures.

Permanent displacements of the rubble mound and the sand layer under the rubble around the deck are plotted against the permanent displacement of the deck in Fig. 24. These displacements were measured from photos taken before and after the shaking. Within the test conditions of this study, the displacement of the deck is proportional to that of the rubble mound. This implies that the deformation of the stiff rubble mound dominated the displacement of deck.

The change of the deformation mode of the ground and the structures can also be seen in Fig. 22 and Fig. 24. The displacement of the caisson became larger than that of the deck in PW2, reflecting the relatively large tilting of the caisson, while in PW7 the tilting of the caisson was small, and horizontal displacements of the deck and the caisson were almost the same, resulting in a small permanent horizontal displacement. Though the thicker liquefiable sand layer made the movement of the overlaying non-liquefiable layer easier, it also made the settlement of the caisson larger. Due to the larger settlement of the caisson, its tilting might have been attenuated, resulting in smaller horizontal displacements of the rubble mound and the deck. Regarding the facts mentioned above, the thicker liquefiable sand layer does not necessarily make the permanent displacement of the deck larger.

The measured strain on the piles just after the shaking in PW2, PW4, PW5 and PW7 are shown in Fig. 25. In PW2, PW5 and PW7, the strain value changed its sign around the sand layer under the rubble. This fact represents that the inflection points in the pile deflection existed at this portion, and there were large relative displacements between the rubble mound and the bearing stratum, as shown in Fig. 23. The strain distribution in PW5 was almost the same in shape as

PW2, but smaller in magnitude. By replacing the backfill with high hydraulic conductivity material to prevent liquefaction, the permanent displacement of the rubble mound as well as the strain on the pile can be reduced. Improvement of the backfill against liquefaction can be an effective countermeasure to prevent the failure of the deck. In case PW4 where the sand layer located under the rubble mound was replaced, the inflection points of the pile deflection were located around the surface of the rubble mound. This confirms that there was no relative displacement between the rubble mound and the bearing stratum. Strains at the pile top in PW4 are smaller than those in the other cases. It can be concluded that improvement of the sand layer under the rubble mound is more effective for reducing the lateral spreading of the ground and preventing the large deformation of piles than improvement of the backfill.

Conclusions

Centrifuge model tests were carried out to investigate the dynamic behaviour of the pile-supported wharf, focusing on the pile-failure mechanism, the effects of liquefaction in the backfill and the sand layer on permanent deformation of the wharf during earthquakes, and the dynamic interaction between the wharf deck and the caisson through the approach bridge. The targeted piled structure was the pile-supported wharf damaged in the 1995 Hyogoken-Nambu Earthquake at Takahama, Kobe. Effects of the model container size, i.e. side boundary conditions, on permanent deformation of the wharf as well as the model ground were also examined by two-dimensional numerical analyses without the piled deck. The following conclusions are drawn:

- The numerical analysis results support that the wharf responses obtained in this study were not much affected by the side walls of the model container, while the distances of the model container side walls from the quay heavily influence the deformation of the ground, since the quay movement is the cause and the deformations of the backfill and the seabed are the consequence. Therefore, determining the width of the analytical domain behind the quay is important and much affects on the piled structure responses when the targeted piled structure is located behind the quay.
- Liquefaction of the foundation soil and the backfill behind the caisson during the earthquake caused a large seaward lateral movement of the rubble mound. As a result, a large horizontal displacement gap was formed between the rubble mound and the bearing stratum. This displacement gap caused very large bending moments at the pile tops and in the bearing stratum just below the sand layer. These large bending moment locations agree with the locations where large pile deformations were observed at the Kobe site. Centrifuge model tests can reasonably predict the failure mode of the piled wharf observed in the Kobe Earthquake.
- Rows of piles are used for stabilisation of a moving slope and this stabilising effect of the rows of piles might have a potential for preventing the movement of the rubble mound and/or the caisson in the tests. However no marked difference can be seen in the displacement distributions of the rubble and the sand layer with or without the pile-supported wharf, since the pile spacing ratio for the pile-supported wharf is relatively large.
- During the shaking, the wharf gradually moved seawards, and no substantial displacement took place after the shaking as no flow liquefaction occurred. This result suggests that not only the deterioration of the soil strength due

to liquefaction but also the continuous cyclic force had a substantial effect on the accumulation of the movement of the wharf.

- The approach bridge connecting the deck of the wharf and the caissons accelerates the seaward movement of the wharf during an earthquake, as the landward movement of the deck is prevented by the caisson through the bridge.
- Variation of thickness of the sand layer under the rubble mound caused a change of deformation mode of the ground and structures. The test without the sand layer beneath the rubble showed no displacement gap between the rubble mound and the bearing stratum, resulting in only a small permanent displacement of the deck, while the thicker liquefiable sand layer did not necessarily cause the larger deformation of the soils and structures.
- Improvement of the liquefiable sand layers is effective to reduce the wharf permanent deformation. Particularly improvement of the sand layer under the rubble mound is more effective for reducing the lateral spreading of the ground and preventing the large deformation of piles than improvement of the backfill.

Acknowledgements

The research presented in this paper was conducted at Tokyo Institute of Technology, Japan and is partially supported by the Japan Association for Steel Pipe Piles. Gratitude is due to the former research student, Mr. Yoshitaka Kawaguchi of Tokyo Gas Company for helping us perform the physical model tests.

References

[1] Technical council on lifeline earthquake engineering of ASCE. 1998. Chapter 2, Experience from past earthquakes, *Seismic guidelines for ports,* TCLEE Monograph No.12, ASCE.

[2] Matsui, T. & Oda, K. 1996. Foundation damage of structures, *Soils and Foundations, Special Issue on Geotechnical Aspects of the Jan. 17 1995 Hyogoken-Nambu Earthquake*, No.1, 189–200.

[3] Tokimatsu, K. & Asaka, Y. 1998. Effects of liquefaction-induced ground displacements on pile performance in the 1995 Hyogoken-Nambu Earthquake, *Soils and Foundations, Special Issue on Geotechnical Aspects of the Jan. 17 1995 Hyogoken-Nambu Earthquake*, No. 2, 163–177.

[4] Egan, J.A., Hayden, R.F., Scheibel, L., Otus, M. and Serventi, G.M. 1992. Seismic repair at Seventh Street Marine Terminal, *Proceedings of the 1992 ASCE Specialty Conference on Grouting, Soil Improvement and Geosynthetics*, Vol.2, 867–878.

[5] Lobedan, F.R., LaBasco, T. & Ogunfunmi, K. 2002. Wharf and embankment strengthening program at the port of Oakland, *Soil Dynamics and Earthquake Engineering*, Vol.22, 1125–1130.

[6] Salah-Mars, S., Arulnathan, R., Roth, W. & Dawson, E. 2004. Seismic evaluation of wharf and embankment at the port of Oakland, California, *Proceedings of the 11th International Conference on Soil Dyanmics and Earthquake Engineering and the 3rd International Conference on Earthquake Geotechnical Engineering*, Vol.2, 813–820.

[7] Japan Association for Steel Pipe Piles. 1995. *Investigative report on steel pipe piles damaged in the 1995 Hyogo-ken Nambu Earthquake* (in Japanese).

[8] Minami, K., Takahashi, K., Yokota, H., Sonoyama, T., Kawabata, N. & Sekiguchi, K. 1997. Investigation results and dynamic response analyses on the damaged 'T' wharf in the Kobe port, *Foundation Engineering and Equipment (Kiso-ko)*, Vol.25, No.9, 112–119 (in Japanese).

[9] Takahashi, K., Minami, K., Yokota, H., Sonoyama, T., Tatsumi, Y. & Noji, M. 1997. Site investigation and static elasto-plastic analyses on the damaged pier in the Kobe port, *Foundation Engineering and Equipment (Kiso-ko)*, Vol.25, No.10, 104–110 (in Japanese).

[10] Sugano, T., Oikawa, K., Santo, M. & Nakahara, T. 1998. Shaking table test on the damaged vertical pile-supported wharf during the 1995 Hyogo-ken Nambu Earthquake, *Proceedings of the 33rd Japan National Conference on Geotechnical Engineering*, Vol.1, 947-948 (in Japanese).

[11] Nishizawa, S., Hashimoto, M., Sakata, Y. & Sonoi, K. 1998. Investigation and analysis of a landing pier of steel pipe piles damaged by the 1995 Hyogoken-Nambu Earthquake, *Soils and Foundations, Special Issue on Geotechnical Aspects of the Jan. 17 1995 Hyogoken-Nambu Earthquake*, No.2, 133–146.

[12] Iai, S. & Sugano, T. 1999. Soil–structure interaction studies through shaking table tests, *Proceedings of the 2nd International Conference on Earthquake Gotechnical Engineering*, Vol.3, 927–940.

[13] McCullough, N.J., Dickenson, S.E. & Schlechter, S.M. 2001a. The seismic performace of piles in waterfront applications, *Proceedings of ASCE Ports 2001 Conference.*

[14] McCullough, N.J., Schlechter, S.M. & Dickenson, S.E. 2001b. Centrifuge modeling of pile-supported wharves for seismic hazards, *Proceedings of Recent Advances in Geotechnical Earthquake Engineering and Soil Dynamics Conference*.

[15] Takahashi, A., Takemura, J., Kawaguchi, Y., Kusakabe, O. & Kawabata, N. 1998. Stability of piled pier subjected to lateral flow of soils during earthquake, *Proceedings of the Centrifuge '98 (IS-Tokyo '98)*, Vol.1, 365–370.

[16] Takahashi, A., Takemura, J., Kawaguchi, Y., Kusakabe, O. & Kimura, T. 1999. Dynamic behaviour of piled pier located in front of gravity type caisson wall during earthquake, *Proceedings of the 11th Asian regional conference on soil mechanics and geotechnical engineering*, Vol.1, 495–498.

[17] Takemura, J., Takahashi, A., Kusakabe, O. & Kimura, T. 1998. Centrifuge model tests on a dynamic stability of piled pier in front of gravity type caisson wall, *Proceedings of the 2nd Japan-UK workshop on implications of recent earthquakes on seismic risk*, TIT/EERG98-6, 111–120.

[18] Takemura, J., Kimura, T., & Suemasa, N. 1989. Development of Earthquake simulators at Tokyo Institute of Technology, *Technical Report, Dept. Civil Engrg. Tokyo Institute of Technology*, No.40, 41–60.

[19] Sakemi, T., Tanaka, M., Higuchi, Y., Kawasaki, K. & Nagura, K. 1995. Permeability of pore fluids in the centrifuge field, *Proceedings of the 10th Asian Regional Conference on Soil Mechanics and Foundation Engineering*, 481–484.

[20] Taylor, R.N. 1995. 2. Centrifuges in modelling: principles and scale effects, *Geotechnical Centrifuge Technology* (ed. Taylor, R.N.), 19–33, Blackie Academic & Professional, London.

[21] Hiro-oka, A., Okamura, M., Takemura, J. & Kimura, T. 1995. Dynamic behaviors of compacted sands surrounded by liquefied loose sand, *Proceedings of the 1st International Conference on Earthquake Geotechnical Engneering*, Vol. 2, 681–686.

[22] Takahashi, A. 2002. Soil–pile interaction in liquefaction-induced lateral spreading of soils, DEng Thesis, Tokyo Institute of Technology.

[23] Takahashi, A. 2003. Seismic performance evaluation of pile-supported wharf by 3D finite element analysis, *Proceedings of the 12th Asian regional conference on soil mechanics and geotechnical engineering*, Vol.1, 245–248.

[24] Hashiguchi, K. & Chen, Z.P. 1998. Elastoplastic constitutive equation of soils with the subloading surface and the rotational hardening. *International Journal for Numerical and Analytical Methods in Geomechanics*, Vol.22, 197–277.

Table 1. Properties of model pile.

Young's modulus, E (GPa)	1.90×10^2
Yield strength, σ_Y (MPa)	2.00×10^2
Pile radius, r (mm)	3.50
Thickness of pipe, t (mm)	0.14
Moment of inertia, I (mm^4)	17.8
Area, A (mm^2)	3.02

Table 2. Material properties of soils used.

	Material	D_{50} (mm)	D_r (%)	Hydraulic conductivity* (m/sec)
Liquefiable sand layer	Toyoura sand	0.19	50	5×10^{-4}
Non-liquefiable sand layer	Silica sand No.3	1.2	75	5×10^{-3}
Rubble mound	Quartz sand	3.1	30	7×10^{-2}
Bearing stratum	Silica sand No.3	1.2	80	5×10^{-3}

$*$: Fresh water was used as pore fluid to measure the hydraulic conductivities.

Table 3. Test conditions.

Case	Input motion	Deck	Approach bridge	Backfill	Sand layer under rubble (Thickness h_s(mm))
PW1	Kobe P.I.	Yes	Yes	◯	◯ (20)
PW2	Sinusoidal	Yes	Yes	◯	◯ (20)
PW3	Sinusoidal	No	No	◯	◯ (20)
PW4	Sinusoidal	Yes	Yes	◯	× (20)
PW5	Sinusoidal	Yes	Yes	×	◯ (20)
PW6	Sinusoidal	Yes	No	◯	◯ (20)
PW7	Sinusoidal	Yes	Yes	◯	◯ (40)

◯ : Liquefiable, × : Non-liquefiable

Table 4. Placed accelerometers and pore pressure transducers in shaking table tests.

Case \ Sensor location	A2	A3	A4	A5	A6	AS1	AS2	AS3	P1	P2	P3	P4	P5	P6
PW1, 2, 4, 5, 6 & 7	◯	×	×	◯	◯	◯	◯	◯	◯	◯	◯	◯	×	×
PW3	◯	◯	◯	◯	◯	◯	◯	×	◯	◯	◯	◯	◯	◯

Table 5. Material parameters for numerical analysis.

Parameter	Sand layer	Rubble mound	Bearing stratum
G_s	2.65	2.69	2.64
e_0	0.79	0.81	0.76
κ	0.0013	0.001	0.0005
λ	0.0072	0.01	0.005
ν	0.33	0.33	0.33
ϕ	40°	47°	45°
ϕ_d	25°	25°	25°
μ	0.9	0.9	0.9
ϕ_b	30°	30°	30°
b_r	100	100	100
u_1	4	9	9
m_1	1	1	1
c	30	30	30
β_{ij0}	$\frac{\sigma_{ij0}-\sigma_{m0}\delta_{ij}}{(-\sigma_{m0})}$	$\frac{\sigma_{ij0}-\sigma_{m0}\delta_{ij}}{(-\sigma_{m0})}$	$\frac{\sigma_{ij0}-\sigma_{m0}\delta_{ij}}{(-\sigma_{m0})}$
$F_0/(-\sigma_{m0})$	1.2	2.4	2.4
s_{ij0}	$0.2\ \sigma_{ij0}$	$0.2\ \sigma_{ij0}$	$0.2\ \sigma_{ij0}$
k (m/s)	1.0×10^{-5}	1.4×10^{-3}	1.0×10^{-4}

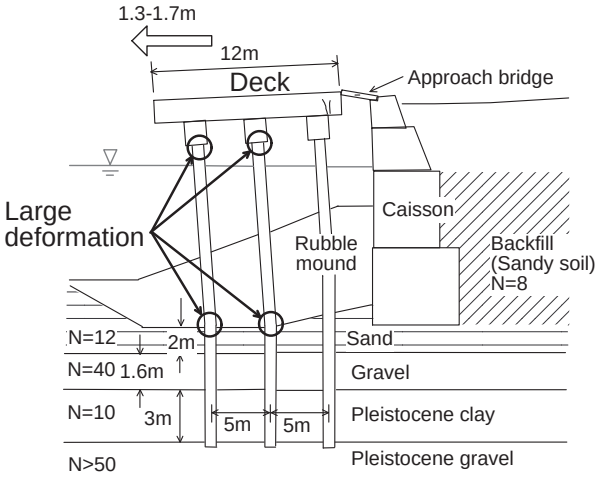

Fig. 1. Cross section of damaged wharf at Takahama, Kobe.

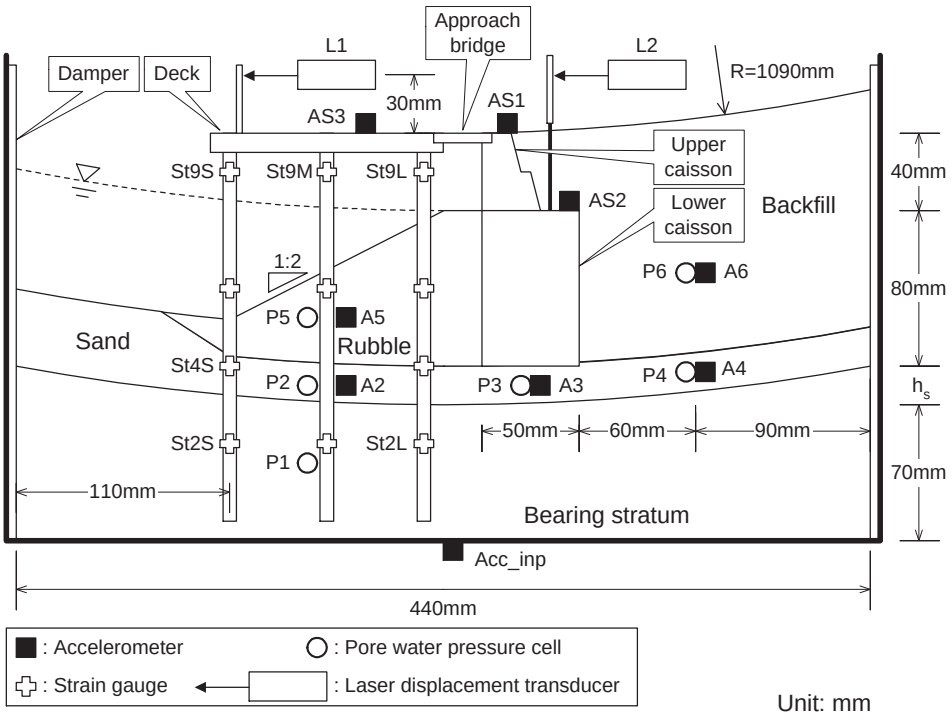

Fig. 2. Model setup for centrifuge tests.

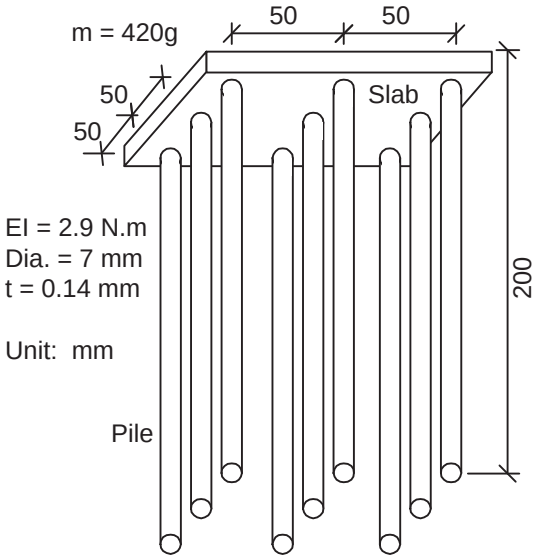

Fig. 3. Detail of a model deck.

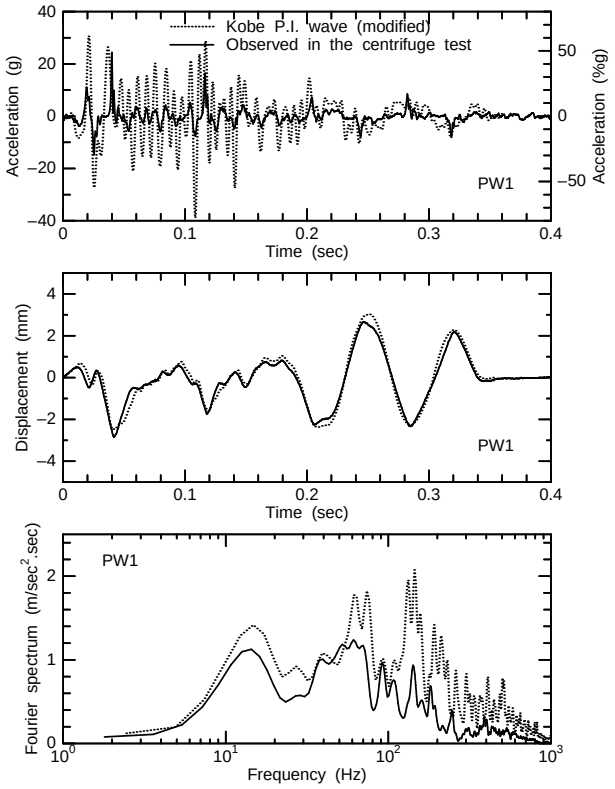

Fig. 4. Time histories of input wave for the Kobe Port Island and Fourier spectra.

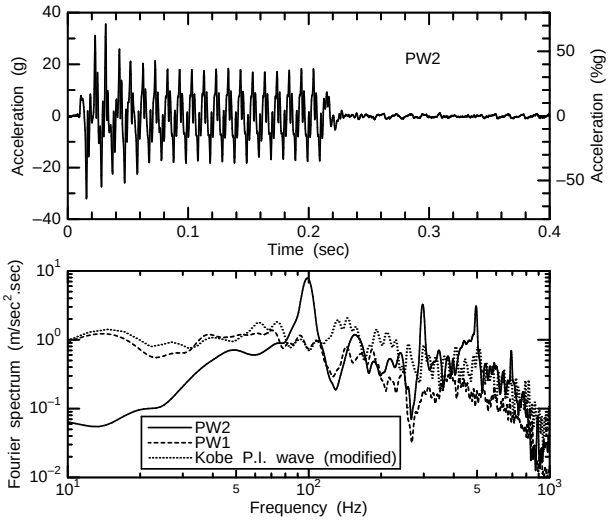

Fig. 5. Time history of input sinusoidal waves and its Fourier spectrum.

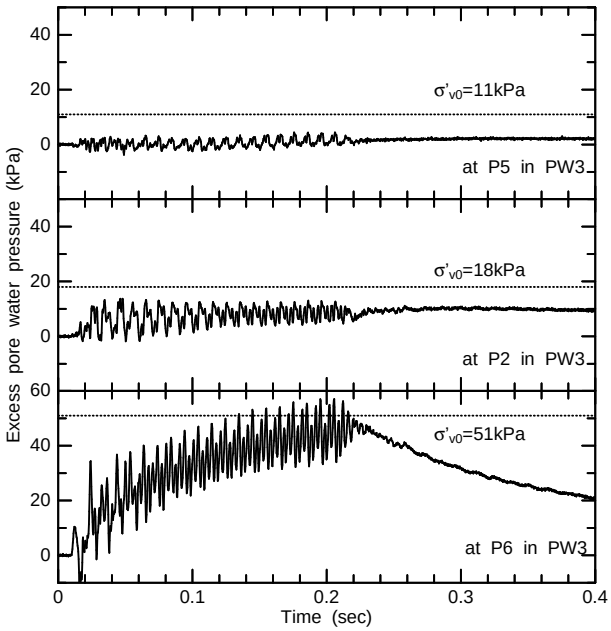

Fig. 6. Time histories of excess pore water pressure at P5, P2 & P6 in PW3.

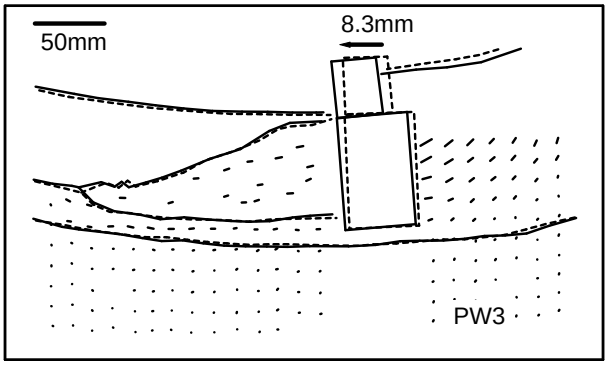

Fig. 7. Observed deformation of model ground in PW3.

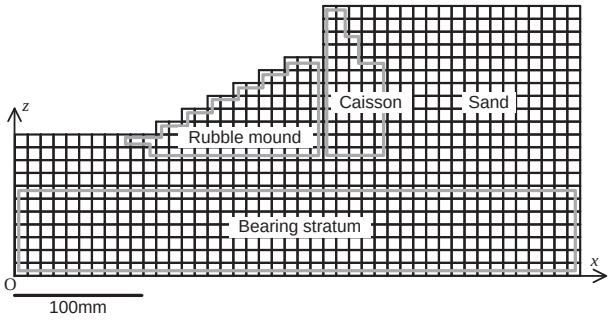

Fig. 8. Finite element mesh for same configuration as centrifuge model tests.

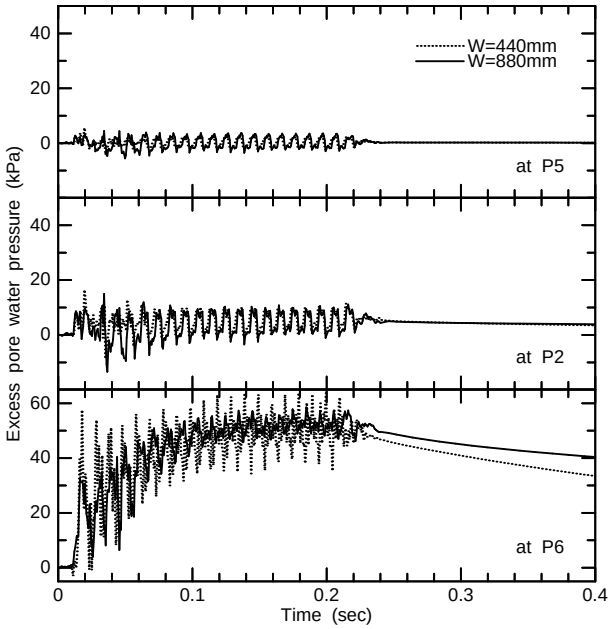

Fig. 9. Calculated time histories of excess pore water pressure.

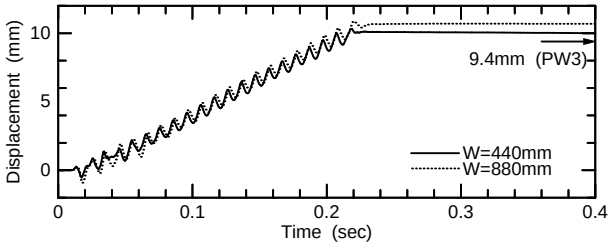

Fig. 10. Calculated time histories of caission displacements.

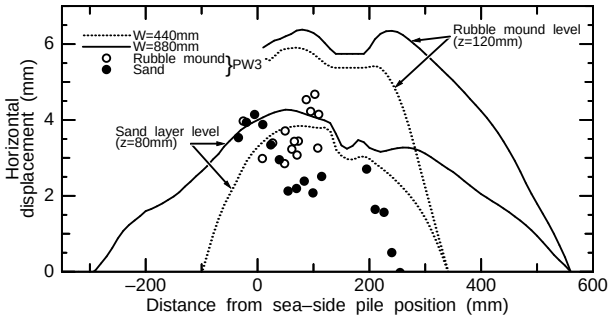

Fig. 11. Permanent horizontal displacement distributions of rubble mound and sand layer under rubble.

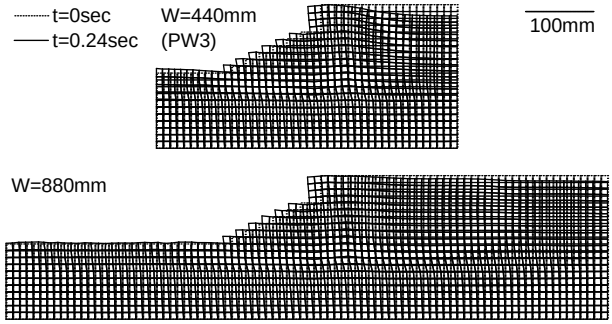

(a) Permanent deformations of model ground at t=0 & 0.24sec.

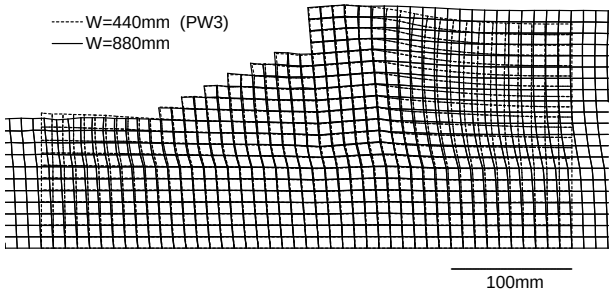

(b) Enlarged permanent deformations of model ground at t=0.24sec.

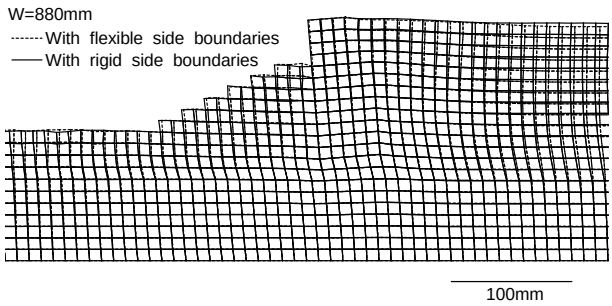

(c) Effects of side boundary conditions on permanent deformation of model ground at t=0.24sec.

Fig. 12. Permanent deformations of model ground in 2D FE analysis, where displacement scale is magnified by a factor of two.

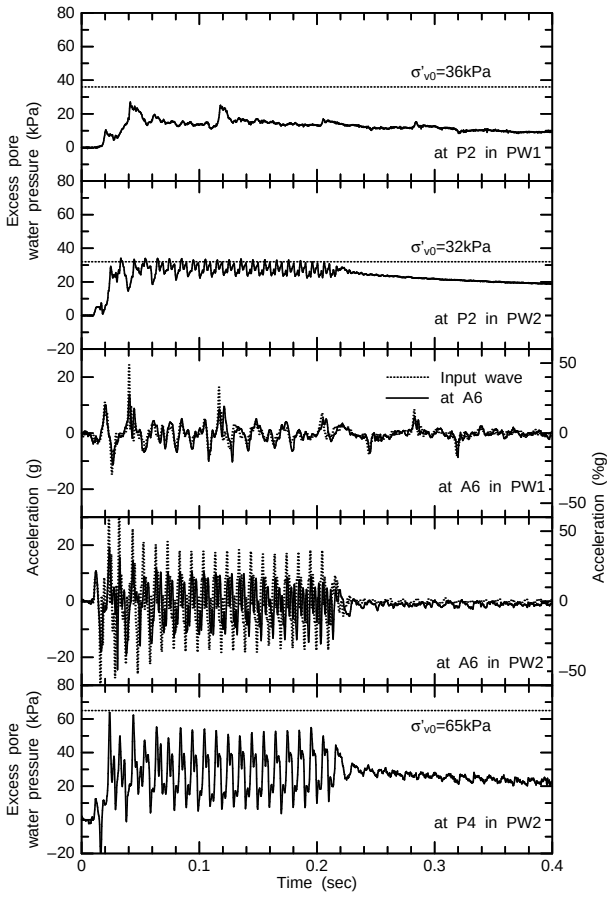

Fig. 13. Time histories of excess pore water pressure at the sand layer, P2 & P4, and acceleration at the backfill, A6, in PW1 & 2.

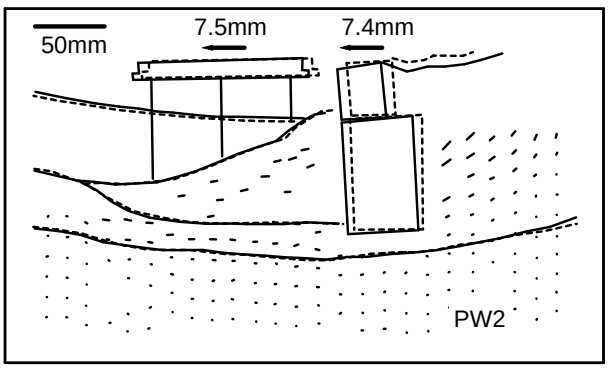

Fig. 14. Observed deformation of model ground in PW2.

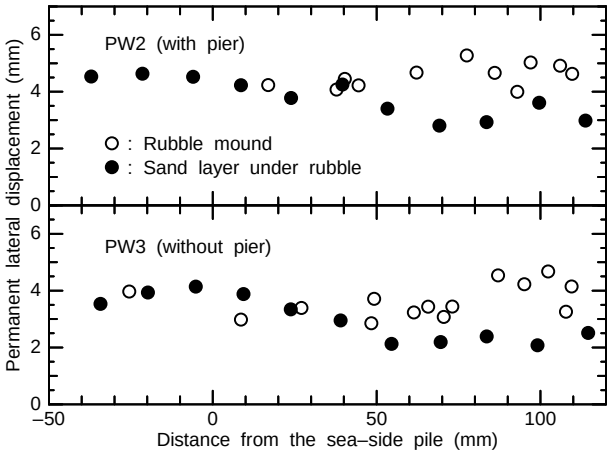

Fig. 15. Permanent lateral displacements of rubble mound and sand layer under rubble in PW2 & 3.

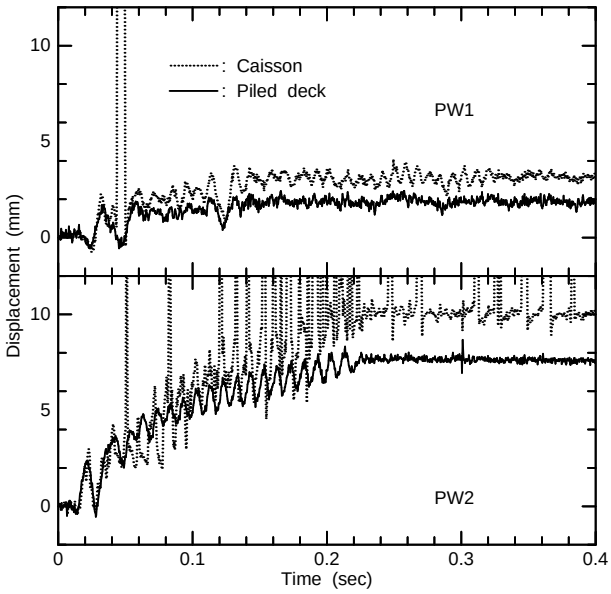

Fig. 16. Time histories of displacements of deck and caisson in PW1 & 2.

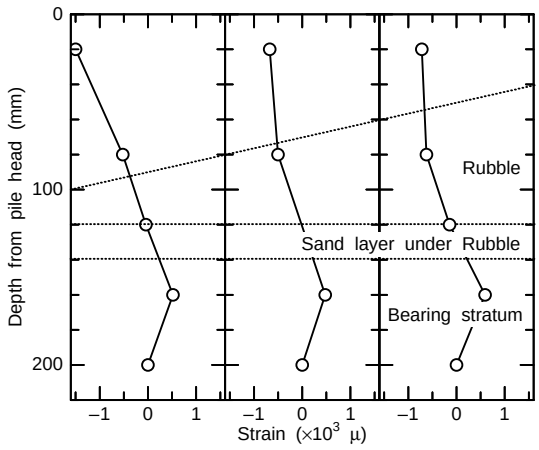

Fig. 17. Permanent strain distributions of pile in PW2.

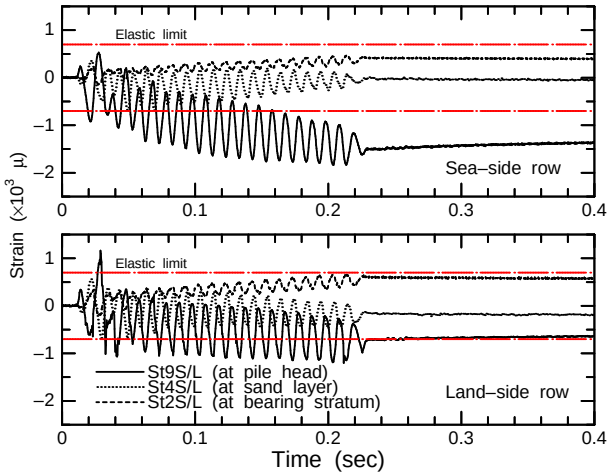

(a) Variations of bending strain in sea-side and land-side rows.

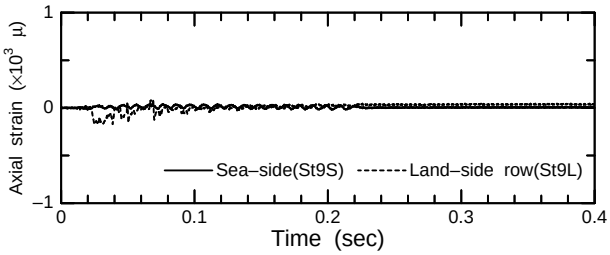

(b) Variations of axial strain at the top of piles.

Fig. 18. Time histories of the strain of pile in PW2.

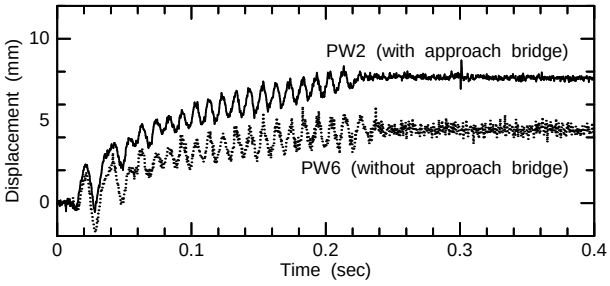

Fig. 19. Time histories of displacement of deck in PW2 & 6.

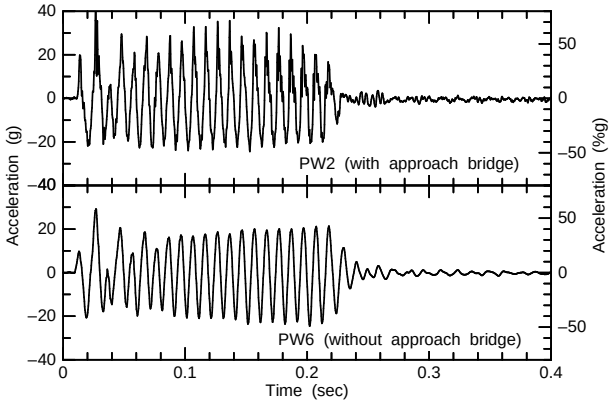

Fig. 20. Acceleration time histories of deck in PW2 & 6.

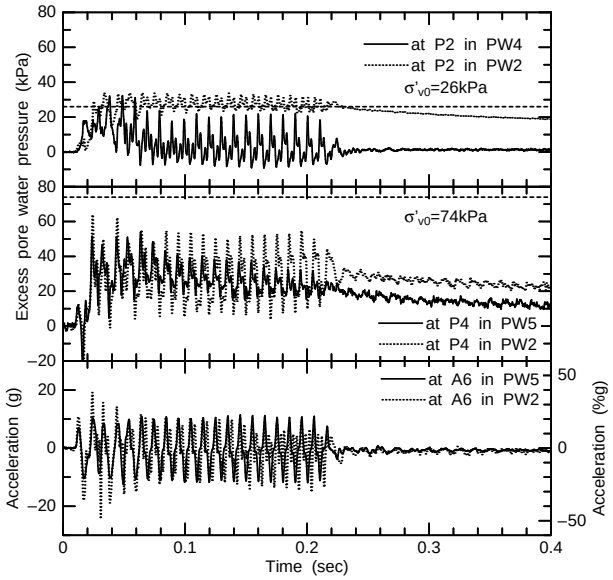

Fig. 21. Time histories of excess pore water pressure at P2 in PW4 and at P4 in PW5 and acceleration at A6 in PW5.

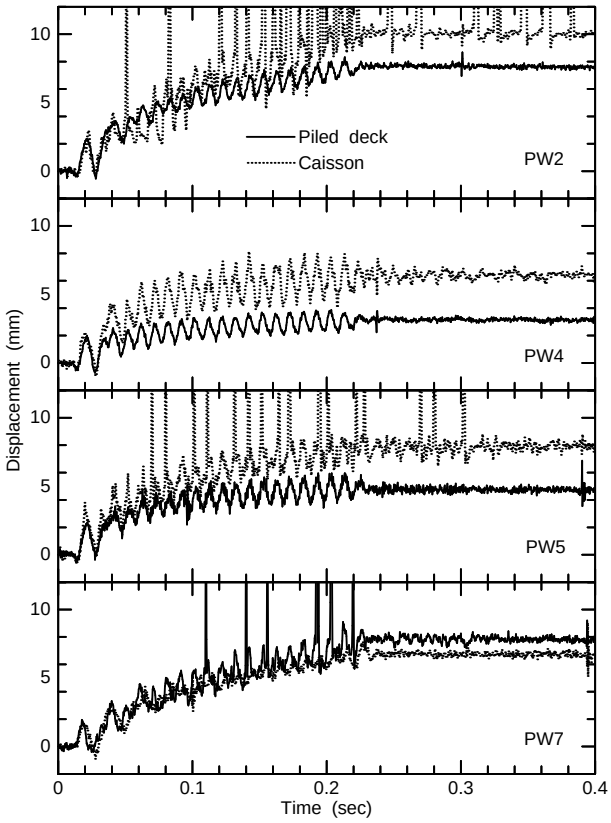

Fig. 22. Time histories of deck and lower caisson in PW2, 4, 5 & 7.

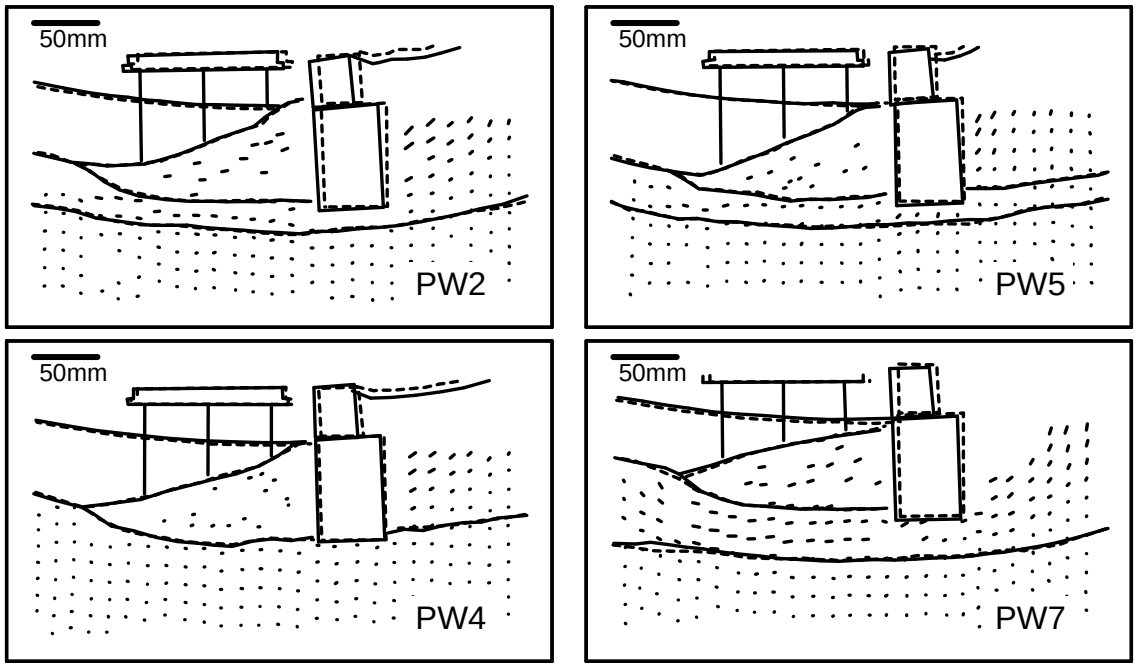

Fig. 23. Permanent deformations of model ground in PW2, 4, 5 & 7.

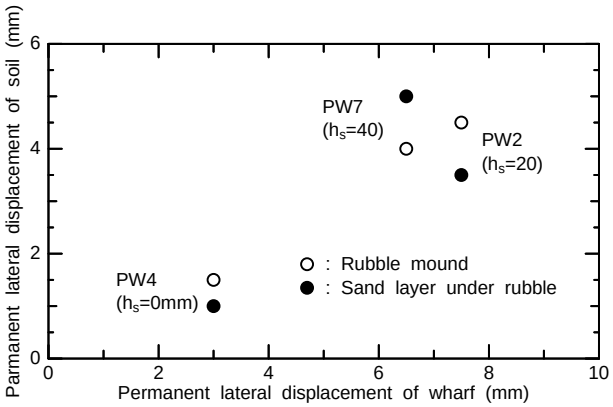

Fig. 24. Permanent lateral displacements of rubble mound and sand layer under rubble against displacement of deck in PW2, 4 & 7.

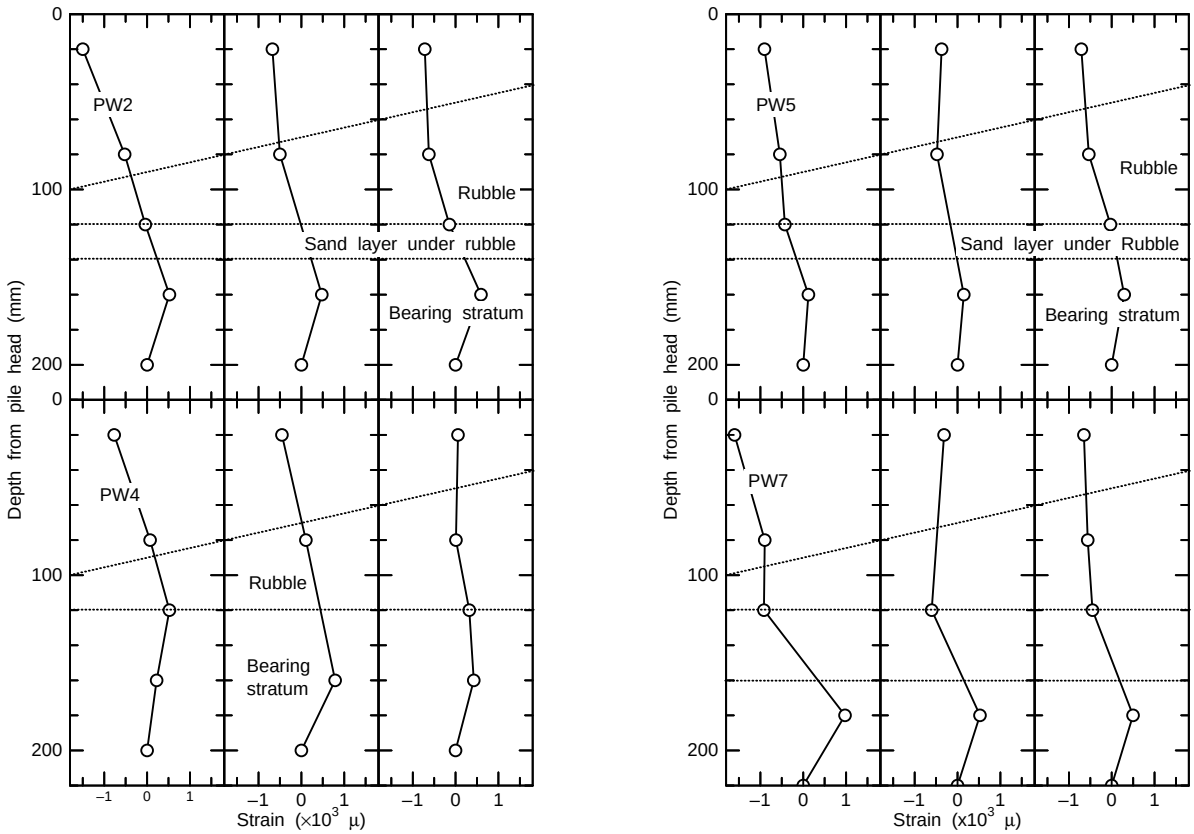

Fig. 25. Distributions of permanent strain of pile in PW2, 4, 5 & 7.